DOI:10.1111/j.1600-0625.2012.01461.x
www.blackwellpublishing.com/EXD

Original Article

Optimization of electron paramagnetic resonance imaging for visualization of human skin melanoma in various stages of invasion

Quentin Godechal[1], Philippe Leveque[1], Liliane Marot[2], Jean-François Baurain[3] and Bernard Gallez[1]

[1]Louvain Drug Research Institute, Biomedical Magnetic Resonance Research Group, Université Catholique de Louvain, Brussels, Belgium; [2]Dermatology Unit, Université Catholique de Louvain, Brussels, Belgium; [3]Medical Oncology Unit, Université Catholique de Louvain, Brussels, Belgium

Correspondence: Bernard Gallez, REMA, Université catholique de Louvain, Avenue Mounier 73.40, B-1200 Brussels, Belgium, Tel.: 32-2-764-73-91, Fax: 32-2-764-73-90, e-mail: bernard.gallez@uclouvain.be

Abstract: Malignant melanoma is a tumor characterized by the uncontrolled proliferation of melanocytes, mainly in skin, but also in eyes. Its incidence is rising each year. To improve the diagnosis and treatment of the tumor, it is essential to develop new effective methods to early detect and characterize melanoma. Previously, we demonstrated in a single-shot study that it was possible to map free radicals of melanin pigments using an electron paramagnetic resonance (EPR)-based method. Furthermore, we demonstrated that X-Band (9 GHz) EPR spectrometry was an accurate tool to assess the growth stage of a pigmented tumor. The aim of the present study was to investigate the ability of EPR imaging to detect and localize melanin pigments inside melanin phantoms, B16 melanoma tumor models and resected human melanomas. We show that EPR can provide an accurate image of synthetic samples, both in terms of shape and size, with errors always lower than 10% compared to the real size. Regarding melanoma studies, the ability of EPR imaging to map accurately the melanoma was depending on the concentration of melanin in the sample, which is proportional to the growth stage of the tumor and the consequent signal-to-noise ratio (SNR) provided by the EPR signal intensity. This led us to define an operational concept, considering SNR and interferences with other EPR signals, to determine when EPR imaging was feasible.

Key words: electron paramagnetic resonance – electron spin resonance – imaging – melanin – melanoma

Accepted for publication 23 January 2012

Introduction

Malignant melanoma is a tumor characterized by the uncontrolled proliferation of melanocytes, mainly in skin. The incidence of this tumor is rising each year (1,2). According to the Surveillance Epidemiology and End Results, skin melanoma is currently the fifth most common cancer diagnosed in men. The last report indicates that in United States., the cumulative lifetime risk for an invasive skin melanoma is estimated at 1/52. This means that 1.93% of American born today will be diagnosed with skin melanoma during their lifetime. Moreover, the mortality of skin melanoma is high, it is the most dangerous form of skin malignancy and it is responsible of three on four deaths linked to a skin tumor (3).

On the other hand, malignant melanoma might appear in other localizations than skin, with a lower incidence. The most common non-cutaneous melanoma is the uveal melanoma with an incidence of 5.3–10.9 cases per million people per year in United States (4). Epidemiological studies show that contrary to that of skin melanoma, the incidence of uveal melanoma stayed stable during the last 30 years (4), with a trend to the decrease (5). Despite the stabilization of its incidence, uveal melanoma remains dangerous because of its aptitude to early metastasization, mainly in liver, lungs and bones. Following the Collaborative Ocular Melanoma Study (COMS) reports, the cumulative rate of metastases at 5 years is 25% (6,7). Metastases in liver are the most frequent and are associated with a median survival of 6 months (8).

Most of the time, diagnosis of both skin and ocular melanomas is difficult. For now, the only methods used for suspecting *in-situ* cutaneous melanoma are visual examination, dermoscopy and digital dermoscopy. These methods, even if effective, show limitations. Indeed, they do not provide any information about the penetration of the tumor in the skin, which is a crucial factor for the determination of the growth state of the potential melanoma, and to provide an adapted treatment. When a tumor is suspected, the lesion is removed and further analysed by histological examination to make a final diagnostic. Although histological examination is an accurate diagnosis tool, it requires a surgical intervention. This intervention may be difficult because the resection margins might appear unclear. Consequently, resection margins are often larger than the visible lesion. However, this is not always sufficient when the melanoma is spreading widely inside the dermis.

The diagnosis of ocular melanoma is also difficult because of the frequent hidden localization of the tumor. All forms of uveal melanoma can usually be suspected *in-situ* with a slit lamp biomicroscopy, but required in-depth examinations using advanced technologies like fluorescein angiography, magnetic resonance imaging, computed tomography or ultrasonography to be confirmed (9). Despite the efficiency of these techniques, none of them is currently able to estimate accurately the tumor penetration, which is crucial information to assess the malignant potential of the suspicious lesion.

For these reasons, it seems essential to improve the diagnosis and treatment of melanoma by developing accurate and non-invasive methods of its detection and characterization. A non-invasive tool could be interesting in assistance to diagnosis of both cutaneous and ocular melanomas and helpful in determining the resection margins on the basis of the invasion depth. Our study takes part in the development of a new magnetic resonance-based method: electron paramagnetic resonance imaging (EPRI).

Electron paramagnetic resonance is a method similar to nuclear magnetic resonance where the electron spins are detected instead of nuclear spins. It has been demonstrated that pigmented melanoma lesions could be detected by EPR spectrometry using the paramagnetic properties of melanin pigments. Indeed, the stable free radicals contained in melanin provide a specific and recognizable EPR signal. The first scientific communication that pointed the EPR properties of melanin was published in Nature in 1954. Commoner had observed an EPR signal in natural melanin which he attributed to free radicals trapped in the pigment (10). This was confirmed a few years later when it was demonstrated that melanins from different origins provided very similar EPR signals (11). Nevertheless, two different signals corresponding to the two major types of melanin, eumelanin and pheomelanin, could be distinguished in ulterior studies (12,13). In 1963, Nebert demonstrated that the melanin contained in melanoma samples was suitable for EPR studies (14). EPR was then successfully applied to the detection and study of synthetic melanins and natural melanins (15–17), but also to different tumor-related samples like paraffin-embedded melanoma slices (18), frozen melanoma samples (14,19,20) and even *in-situ* melanomas (21). The sensitivity of the method was proven by comparison with other well-documented methods like high-performance liquid chromatography (13), and the ability of using EPR method to quantify melanin on the ground of the amplitude of its spectrum was also demonstrated (22,23). In 2005, Timmins (24) submitted a patent for the concept of detecting melanoma by EPR, and recently, our team demonstrated that there was a correlation between the amplitude of the melanin signal coming from an experimental melanoma and the growth stage of the tumor (25).

On the other hand, Katsuda demonstrated that it was possible to get an image from an *ex-vivo* melanoma using a X-band (9 GHz) EPR spectrometer (26), and in 2008, our group was able to get the first image of melanin pigments from an *in-situ* B16 mouse melanoma using an L-band (1 GHz) EPR spectrometer (27).

For more information, the field of applications of EPR to skin and hair research has recently been reviewed by Plonka (28).

It is now established that EPR spectrometry can successfully be used to detect melanin inside pigmented melanoma. However, the spectrometry technique does not provide any spatial information about the repartition of pigments inside the sample. This information would be very helpful to assess the size and the depth penetration of melanomas, which are critical characteristics for the diagnosis, the definition of the margins for tumor resection and the monitoring of the tumor progression. In the present work, we investigated the ability of EPR imaging to detect and map the melanin pigments inside different kinds of samples relevant for melanoma studies. The study started with synthetic melanin samples mimicking melanoma with different Clark index (invasiveness into the skin), then moved to mouse melanomas and finally to human skin melanomas. The main objective of this work was to determine the level of accuracy and the detection limit of EPR imaging when applied to melanin-containing samples like human pigmented melanoma.

Materials and methods

Samples preparation

Synthetic phantoms mimicking melanoma

Three synthetic phantoms (S1, S2 and S3) were moulded with synthetic eumelanin (cell culture tested synthetic melanin; Sigma-Aldrich, GmBh, Steinheim, Germany) diluted in D-Sucrose with concentration 1/10 w/w. These phantoms were created in the 'T' shape of typical melanoma, where the horizontal and transversal bars of 'T', respectively, refer to the radial and vertical growth phase of the tumor. The dimensions of the samples were measured using a calliper and ranged from 4.8 mm (horizontal) × 2.6 mm (vertical) to 6.6 mm × 4.4 mm. The cross-section was identical from one sample to another (0.7 mm) and homogenous so that the quantity of melanin was equal from the edges to the centre. These samples were coated with non-paramagnetic tape, so that melanin could not move during the measurements, and put into a quartz tissue cell (ER 162 TC-Q Tissue Cell; Bruker Biospin, GmBh, Rheinstetten, Germany).

Mouse melanoma samples

B16F10 melanoma cells were routinely cultured in serum-containing DMEM. 750 000 melanoma cells were injected s.c. to 8-week-old male C57Bl6 mice ($n = 3$; Elevage Janvier, France). Animals were sacrificed and tumors excised 8 days after injection. The first tumor was freeze-dried and one 1-mm-thick slice was cut and coated with non-paramagnetic tape. This slice was used as a sample and put into a quartz tube at the time of measurement. The two other tumors were fixed using Bouin's fixative, a solution composed of formol, picric acid and acetic acid, and then embedded with paraffin. Two hundred-and 100-μm-thick slices were cut from each of these two tumors. These samples were put into a flat quartz tissue cell at the time of measurement. As a control, Bouin's fixative and paraffin were measured alone by EPR spectrometry using the same parameters.

Human melanoma samples

Specimens of human cutaneous melanomas were obtained from the melanoma bank of the Dermatology Unit of the 'Cliniques Universitaires Saint-Luc' in Brussels, Belgium. The melanomas were classified into four categories in function of their Breslow index (index for evaluating the tumor thickness) at the time of excision and following the AJCC 2001 classification system.

- T4 ($n = 3$) means that at the time of excision, these melanomas were in an advanced growth stage, with the possible presence of satellite metastases around the tumor. The primary lesion was invading the subcutaneous tissues and/or had a thickness higher than 4 mm.
- T3 ($n = 3$) means that, at the time of excision, these melanomas were invading the papillar dermis, the reticular dermis and/or had a thickness ranging between 2 and 4 mm.
- T2 ($n = 3$) means that the tumors were invading the papillar dermis, the reticulo-papillar junction and/or had a thickness ranging between 1 and 2 mm.

• T1 (n = 3) means that the tumors were only invading the papillary dermis and had a thickness inferior to 1 mm.

All tumors were fixed with Bouin's fixative and embedded in paraffin. A 500-μm-thick slice was cut from each tumor and used as a sample. All samples were put into a flat quartz tissue cell at the time of measurement.

All experiments were approved by the local ethics committee (N/ref. 2010/12AVR/120 – No. B40320108558).

EPR measurements

All spectra and images were recorded at room temperature on a Bruker E540 Elexsys system (Bruker Biospin, GmBh) equipped with a Super High Sensitivity Probe (10mm diameter, 30 mm long) operating in X-band mode at approximately 9.5 GHz and 100 KHz modulation frequency. Parameters were chosen to provide the best signal-to-noise ratio (SNR) with no distortion of the signal shape. For images, the following parameters were used: microwave power: 3.2 mW; modulation amplitude: 0.25 mT; conversion time: 10.24 ms; time constant: 5.12 ms; sweep width: 100 G; number of points: 1024; number of scans: 40; sweep time: 41.94 s; gradient field: 450 mT/m; number of projections: 25; pixel size: 0.6 mm; total acquisition time: 18.5 min. The spectra were acquired in the same conditions, in the absence of gradient field. Image and spectrum acquisitions were repeated three times for every sample. 2D images were reconstructed on a 128 × 128 matrix by filtered backprojection using a Shepp–Logan filter. Before reconstruction, each projection was deconvoluted using fast Fourier transform with the measured zero-gradient spectrum to improve image resolution. To reduce noise amplification and avoid possible division by zero at high frequencies, a low pass filter was used. The deconvolution parameters, including the maximum cut-off frequency and the width of the window in the Fourier space, were set-up after viewing the shape of all projections. Data were smoothed using a Gaussian filter. Spectral deconvolution and filtered backprojection were performed using the Xepr software package (Bruker). Dimensions of the samples on EPR images were measured using a dedicated application in the Bruker Elexsys software. For each image, a reference spectrum was obtained at the same parameters so that SNR could be measured.

Results

Synthetic melanin phantoms

The three samples made of synthetic melanin were first measured using EPR imaging. For each sample (S1, S2, S3), real dimensions and dimensions measured on the image are summarized in the Table S1. We observed that dimensions on the images were always correlated to the real dimensions, with differences between them always <10% of the real size. Pictures of the three samples with their associated EPR image are shown on Fig. 1. It was observed that the shape of the samples was corresponding to the real samples and that intensity of EPR signal was homogenous. The loss of intensity towards the edges of the object (the so-called 'edge effect') reflects the finite resolution which is limited by the spectral properties of melanin. A reference spectrum was obtained from each of the three samples. The SNRs measured on these spectra were ranging from 106.7 for the biggest sample (S1) to 73.3 for the smallest sample (S3). As demonstrated in a previous study, the SNR is tightly linked to the quantity of melanin inside the sample (25).

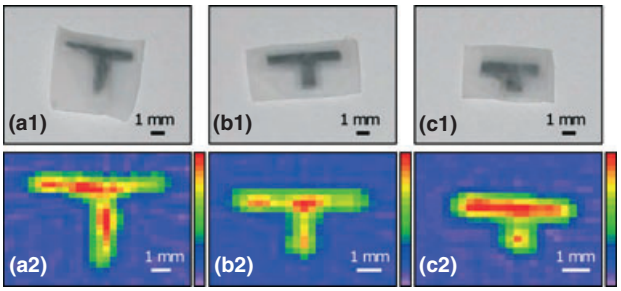

Figure 1. Synthetic phantoms: Three synthetic phantoms made with synthetic melanin diluted in D-sucrose (concentration 1/10), from the left to the right: S1 (a.1), S2 (b.1) and S3 (c.1), and their respective electron paramagnetic resonance (EPR) images (a.2, b.2, c.2). For samples and images dimensions, refer to the Table S1.

Mouse melanoma

Five mouse melanoma samples were then measured and imaged using X-Band EPR. A summary of the results can be found in the Table S1. The 1-mm-thick freeze-dried sample (M1) and the two 200-μm-thick paraffin-embedded samples (M2, M3) provided accurate EPR images in which general shapes correlated with the real shapes (Fig. 2) and the differences between real sizes and image sizes did not exceed 10% of the real size. As we can see, especially on the image of M1, the signal intensity was slightly less homogeneous than in synthetic samples. This could be explained by an inhomogeneous repartition of the melanin pigments inside the samples. As for synthetic phantoms, a reference spectrum was obtained from each sample. These EPR spectra were characterized by the presence of one single-line signal corresponding to the eumelanin signal. The SNR observable on the spectra was ranging from 75.2 for M1 to 26.3 for M3.

The other two mice melanoma samples were 100 μm-thickness slices (M4, M5), coming from the same tumors as M2 and M3, and contiguous to them. As we can see on Fig. 2.b.3,c.3, these two

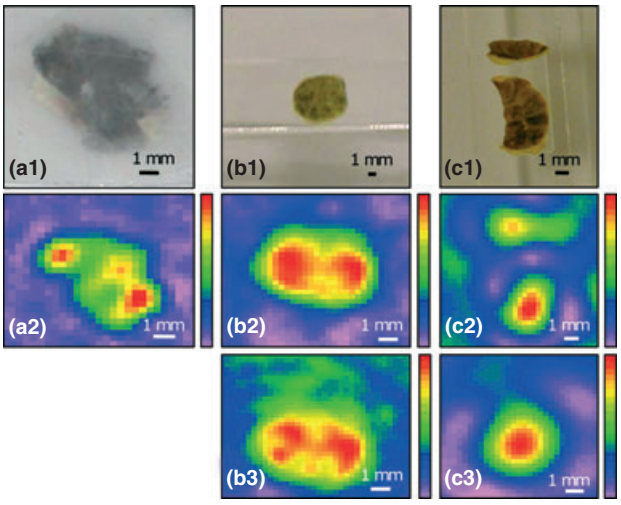

Figure 2. Mouse melanoma: Three mouse B16 melanoma samples, from the left to the right: M1 (a.1), M2 (b.1) and M3 (c.1). M1 is a 1-mm-thick slice from a freeze-dried melanoma. Its electron paramagnetic resonance (EPR) image is shown on figure a.2. M2 and M3 are 200-μm-thick slices from paraffin-embedded melanomas. Their respective EPR images are shown in figures b.2 and c.2. Figures b.3 and c.3 show EPR images of 100-μm-thick slices contiguous to M2 and M3 (M4 and M5). For samples and images dimensions, refer to the Table S1.

samples did not allow the acquisition of clear images. The measurement of the vertical dimension of the M4 image was not possible and the sample M5 provided a rough image, with a unique central spot while the real sample was composed of two parts. Consequently, it was not relevant to get measurements of the size of these two samples. A reference spectrum was obtained from each sample, showing a SNR of 8.2 for M4 and 7.3 for M5. These values were weaker than for the first three samples, which was the consequence of the lower thickness of the slices and so, the lower quantity of melanin inside the EPR cavity.

Human melanoma

Twelve human melanoma samples were measured, beginning with three 500 μm-thickness slices coming from melanomas classified as T4 by anatomopathologists (H1, H2, H3). The dimensions of the samples and their respective images are indicated in the Table S1. For each of these three samples, we observed that real dimensions and dimensions of their images were correlated, with differences between them not exceeding 10%. As we can see on the Fig. 3, the real shapes and shapes of the images were corresponding, but the EPR intensity inside the images was not homogeneous. This inhomogeneity of the intensity could be correlated with inhomogeneities of thickness for H1 and inhomogeneity of pigmentation for H2 an H3. As for synthetic samples and mouse melanomas, a reference spectrum was obtained from each human sample. For these three T4 samples, the SNR was ranging from 1107.2 for H1 to 21.7. This big difference of SNR could be explained by the difference of size and pigmentation between the samples.

The next three human melanoma samples came from T3 tumors (H4, H5, H6) (Fig. 4). It was pointed that only the sample H4 (Fig. 4.a.1) could provide an EPR image. This image was fairly correlated with the real sample, showing a decrease in intensity in the lower part that could be associated with a decrease in the pigmentation in the same area. The two other samples, H5 and H6, did not allow the reconstruction of any EPR image. An EPR reference spectrum was obtained from the samples and a slight difference was observed between their respective SNR's. Indeed, the spectrum coming from the imageable sample presented a SNR of 11.0, while the two other samples presented SNR's of 6.5 and 2.5, which consequently seemed insufficient for EPR imaging. A second notable difference was found between the spectrum of H4 and the two other spectra that can be explained the difficulty to get an image from those samples: the appearance of an unknown EPR signal, different from melanin signal, and positioning next to it. The g-factor of this signal was $g = 2.230$ for H5 and $g = 2.337$ for H6. To allow the reconstruction of an EPR image, the baseline of the reference spectrum must be flat, which was not the case here, as we can see on Fig. 4.b.2,c.2.

Like the two previous samples, the last six samples of the study, coming from T2 melanomas (H7, H8, H9) and T1 melanomas (H10, H11, H12), did not allow the reconstruction of any EPR image. The SNR were measured on the reference spectrum of each sample and were ranging from 6.3 to 1.8, with a mean SNR slightly higher for samples coming from T2 stages. Moreover, an interfering EPR signal was observed on five of the six spectra.

It must be noted that, when looking at the spectra of the human samples, the EPR signal mostly referred to eumelanin, characterized by a single line spectrum, with a negligible contribution of pheomelanin, characterized by a ^{14}N hyperfine-splitted free radical signal consisting of three features, the high-field one hardly read-

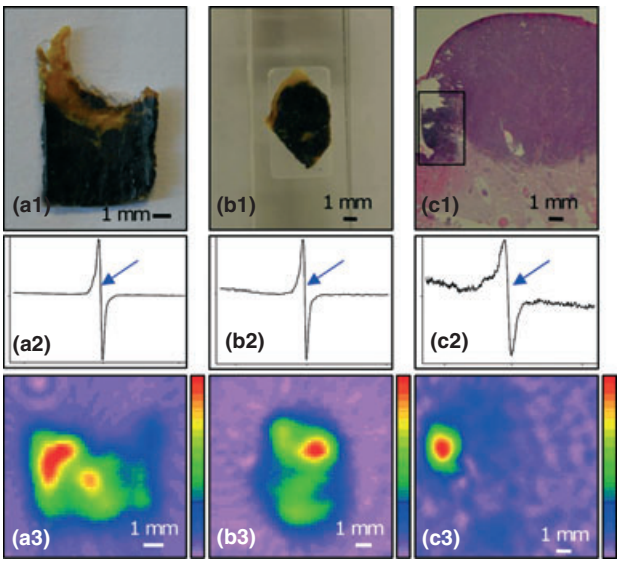

Figure 3. T4-stage human melanoma: 500-μm-thick slices were cut from three paraffin-embedded T4-stage human melanomas. From the left to the right: samples H1 (a.1), H2 (b.1) and H3 (c.1). For sample H3, an histological section is presented. Electron paramagnetic resonance (EPR) spectra recorded from these samples are shown in figures a.2, b.2 and c.2. The EPR signal of melanin ($g = 2.005$, linewidth = 0.55 mT) is pointed (blue arrow) on every sample. EPR images obtained from these samples are shown in figures a.3, b.3 and c.3. For dimensions, refer to the Table S1.

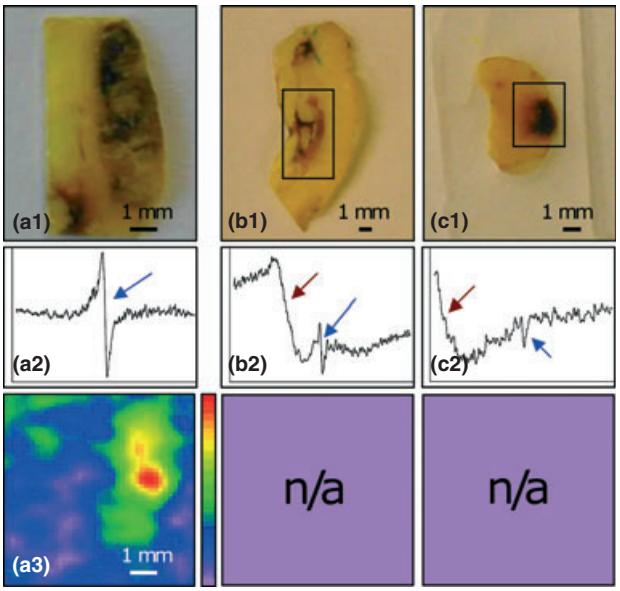

Figure 4. T3-stage human melanoma: 500 μm-thickness slices were cut from three paraffin-embedded T3-stage human melanomas. From the left to the right: samples H4 (a.1), H5 (a.2) and H6 (a.3). Electron paramagnetic resonance (EPR) spectra recorded from these samples are shown in figures a.2, b.2 and c.2. The EPR signal of melanin ($g = 2.005$, linewidth = 0.55 mT; blue arrow) and interfering signals ($g = 2.230$, linewidth = 10.6 mT for H5; $g = 2.337$, linewidth = 26.7 mT for H6; red arrow) are pointed. The EPR image of sample H4 is shown on figure a.3. No EPR image could be reconstructed from H5 or H6 sample. For samples and images dimensions, refer to the Table S1.

able (12). However, the presence of pheomelanin was more pronounced for c and d samples (see Figure S1), confirming the possibility that melanoma might contain the both types of melanin in variable concentrations (29,30). The main line on these spectra was slightly wider (0.70 mT) compared with pure eumelanin spectra (0.55 mT), which is a characteristic of the presence of pheomelanin (31).

Discussion

In this work, it was demonstrated that EPR imaging could detect and provide accurate information about the dimensions of melanin-containing samples. Indeed, the images obtained from the three synthetic phantoms were faithful to the real samples, both in terms of shapes and dimensions. However, minor differences between real sizes and image sizes were observed (max = 0.2 mm). Explanations to this phenomenon were firstly the gradient field limitation (max = 450 mT/m) that led to a resolution limitation because the maximum theoretical resolution is determined by the ratio between the linewidth of the EPR signal and the applied gradient field (0.55 mT/450 mT $\times$ m^{-1} = 0.0012 m). However, in practical terms, this resolution is improved by the deconvolution process. Secondly, these small differences were also because of the difficulty to obtain absolutely accurate measurements when using the calliper or the measurement software. Another observation that could be pointed out was the heterogeneity of the intensity inside images obtained from these homogenous synthetic phantoms. Indeed, non-initiated eye might have expected a totally homogenous intensity all over the samples. However, a decrease in the signal around the edges of images was observed. This phenomenon is very classical and merely reflects the limited resolution of the technique resulting in somewhat blurry edges rather than sharp and clear cut edges. Nevertheless, the deconvolution process used before image reconstruction attenuated this limitation.

The observation of the results obtained from mouse melanomas pointed another limitation to the method. In the biological samples, it was already demonstrated that the concentration of melanin was lower than in this kind of synthetic phantoms and was correlating with the tumor growth state (25). Therefore, a decrease in the SNR was awaited, leading to a lower quality of images, especially for small tumor samples. This phenomenon was observed, with the consequence that the two thinnest samples (100 μm) could not provide any EPR image. As a characteristic of the melanin contained in the samples, the SNR was measured on every reference spectrum. As expected, it was observed that the two 100 μm-thickness slices had the lowest SNR's of this group of samples with 8.2 and 7.3, while the three thicker samples were 75.2, 30.9 and 26.3. From this observation, we could determine that, in the absence of any interfering signal, the threshold to apply successfully EPR imaging to melanin-containing samples was situated between 8.2 and 26.3.

The final part of the study, focusing on the detection of human melanoma, was somehow the most interesting. Despite the limits of the method, which will be discussed later, it was demonstrated that there was a link between the ability to get clear EPR images and the tumor invasion state. This confirmed the results obtained in our previous study, where it was observed that there was a straight correlation between the tumor growth stage and the SNR of the EPR spectrum (25). Moreover, the link between the SNR and the ability to use EPR imaging observed for mouse melanoma was here confirmed. Indeed, while the T4-stage samples were perfectly convenient for EPR imaging, the acquisition of images from tumors with inferior grades was more difficult. In fact, amongst the three T3 melanoma samples, only one allowed the reconstruction of a clear EPR image. This sample had a SNR of 11.0 when the two non-imageable samples had SNR's of only 6.5 and 2.5. In the same way, EPR imaging was not feasible for T2 and T1 samples where the SNR's were comprised between 6.3 and 1.8. By associating results for human and mouse melanoma, we could refine the limit of application of EPR imaging to melanin-containing samples that provide SNR's ranging between 11.0 and 8.5 in the absence of interfering signals. However, interfering signals appeared clearly on two of the three T3-stage melanomas and five of the six T2 and T1-stage melanomas and constituted an additional barrier to the successful application of EPR imaging to early melanomas. The origin of these signals has not been determined so far. Nevertheless, it has been demonstrated in the literature that metal ions could be adsorbed by melanin (32) and that the presence of metal ions had a direct consequence on the saturability of melanin signal (16). Considering this information, a complementary experiment was performed to compare the microwave power saturability of samples that present an interfering signal and those that do not. It was shown that samples presenting an interfering signal were harder to saturate with microwave power than others. This observation is in line with the previous references and lets us think that the interfering signals may be linked to the presence of metal ions inside a part of the melanoma samples.

As a conclusion, we demonstrated for the first time that EPR X-Band imaging could provide accurate and specific images of human melanoma samples, despite some indubitable actual limits. This was achieved by focusing the measurements on the EPR signal of melanin pigments. However, it must be noted that amelanotic melanomas exist and will thus never be detectable by this method. In the same way, there is still no means of distinguishing melanoma from a benign melanocytic nevus.

For now, the most effective tools to diagnose melanoma remain dermoscopy, followed by histological examination if necessary. Because of the actual limits in sensitivity and resolution of X-Band EPR, and because the problem of sensitivity will be still more pronounced *in-vivo* in L-Band, dermoscopy stays incontrovertible. In fact, this method is the most accurate to define *in-vivo* the border of the tumor, its shape, fragmentation and its fractal dimension, which is one of the most straightforward parameter determining the invasiveness of the tumor. On the other hand, anatomopathology remains the most efficient tool to confirm the diagnosis and estimate the expanse of the tumor without performing a complete resection. Nevertheless, the interest of developing an EPR-based method applicable *in-vivo* is still high. The ability of EPR imaging to detect and map melanin pigments would be very helpful in the case of ocular melanomas, where the tumor is generally hidden. In the field of skin melanoma treatment, EPRI could also play a role by determining non-invasively the expanse of melanoma widespread inside of the skin and determine the margins of resection for excision, which is for now impossible without performing one or more biopsies. For that purpose, upgrading the sensitivity of EPR method is necessary. The use of S-Band EPR should be considered (28). In fact, the sensitivity of this method is higher than L-Band but lower than X-Band, but microwaves may only pene-

trate 3–4 mm inside of a water-containing sample like skin, which might be insufficient for big tumors. On the other hand, technical improvements, especially in the field of EPR cavities and postprocessing treatment of spectra and images, are on the way (33,34) and should, in the future, enhance the performance of both *ex-vivo* and *in-vivo* EPR.

Acknowledgements

This work is supported by grants from the Belgian National Fund for Scientific Research (FNRS), the Televie, the Fonds Joseph Maisin, the Saint-Luc Foundation, the 'Actions de Recherches Concertées-Communauté Française de Belgique-ARC 09/14-020', the Fondation contre le Cancer, and the ' Pôle d'attraction Interuniversitaire PAI VI (P6/38)'.

Author contributions

Godechal performed the research, analysed the data and wrote the paper. Levêque contributed to the analysis of the data and the drafting of the paper. Marot and Baurain provided the human melanoma samples and contributed to the analysis of the data. Gallez designed the research, contributed to the analysis of the data and the drafting of the paper.

Conflict of interests

The authors have declared no conflicting interests.

References

1 Woodhead A D, Setlow R B, Tanaka M. J Epidemiol 1999: **9**: 102–114.
2 Linos E, Swetter S M, Cockburn M G *et al.* J Invest Dermatol 2009: **129**: 1666–1674.
3 Jerant A F, Johnson J T, Sheridan C D *et al.* Am Fam Physician 2000: **62**: 357–368.
4 Singh A D, Topham A. Ophthalmology 2003: **110**: 956–961.
5 Inskip P D, Devesa S S, Fraumeni J F Jr. Cancer Causes Control 2003: **14**: 251–257.
6 Willson J K V, Albert D M, Diener-West M *et al.* Arch Ophtalmol 2001: **119**: 670–676.
7 Diener-West M, Reynolds S M, Agugliaro D J *et al.* J Clin Oncol 2004: **22**: 2438–2444.
8 Kim I K, Lane A M, Gragoudas E S. Arch Ophtalmol 2010: **128**: 871–875.
9 Papastefanou V P, Cohen V M L. J Skin Cancer 2011: **2011**: 573974.
10 Commoner B, Townsend J, Pake G. Nature 1954: **174**: 689.
11 Mason H S, Ingram D J E, Allen B. Arch Biochem Biophys 1960: **86**: 225.
12 Sealy R C, Hyde J S, Felix C C *et al.* Science 1982: **217**: 545–547.
13 Vsevolodov E B, Ito S, Wakamatsu K *et al.* Pigment Cell Res 1991: **4**: 30–34.
14 Nebert D W, Mason H S. Cancer Res 1963: **23**: 833–840.
15 Hansson C, Rosengren E. Acta Derm Venereol 1979: **59**: 175–176.
16 Okazaki M, Kuwata K, Miki Y *et al.* Arch Biochem Biophys 1985: **242**: 197–205.
17 Enochs M S, Nilges M J, Swartz H M. Pigment Cell Res 1993: **6**: 91–99.
18 Elek G, Lapis K, Rockenbauer A. Br J Cancer 1980: **41**: 199–203.
19 Atlas S W, Braffman B H, LoBrutto R *et al.* J Comput Assist Tomogr 1990: **14**: 547–554.
20 Plonka P M, Slominski A T, Pajak S *et al.* Exp Dermatol 2003: **12**: 356–364.
21 Lukiewicz S J, Lukiewicz S G. In-vivo ESR spectroscopy of pigmented tumors in mice. The XIIth International Pigment Cell Conference. Giessen, Germany, 1983: 133.
22 Pilas B, Sarna T. Quantitative determination of melanin in pigmented cells by electron spin resonance spectroscopy. In: Bagnara J, Klaus S N, Paul E, Schartl M, eds. Pigment Cell 1985. Biological, Molecular, and Clinical Aspects of Pigmentation. Tokyo: University of Tokyo Press, 1985: 97–103.
23 Cieszka K A, Hill H Z, Hill G J *et al.* Exp Dermatol 1995: **4** (4 Pt 1): 192–198.
24 Timmins G S. Detecting melanoma by electron paramagnetic resonance. US patent application 2005/0288573 A1.
25 Godechal Q, Defresne F, Danhier P *et al.* Contrast Media Mol Imaging 2011: **6**: 282–288.
26 Katsuda H, Kobayashi T, Saito H *et al.* Chem Pharm Bull (Tokyo) 1990: **38**: 2838–2840.
27 Vanea E, Charlier N, DeWever J *et al.* NMR Biomed 2008: **21**: 296–300.
28 Plonka P M. Exp Dermatol 2009: **18**: 472–484.
29 Prota G, Rorsman H, Rosengren A-M *et al.* Experientia 1976: **32**: 970–971.
30 Morishima T, Fukada E. Arch Dermatol Res 1985: **277**: 248–250.
31 Slominski A, Plonka P M, Pisarchik A *et al.* Endocrinology 2005: **146**: 1245–1253.
32 Sarna T, Hyde J S, Swartz H M. Science 1976: **192**: 1132–1134.
33 Brinton C G, Hirsh D J. Rev Sci Instrum 2010: **81**: 026102.
34 Ikebata Y, Sato-Akaba H, Abyama T *et al.* Magn Reson Med 2009: **62**: 788–795.

Supporting Information

Additional Supporting Information may be found in the online version of this article:

Figure S1. Electron paramagnetic resonance spectrum of the human melanoma sample H3.

Table S1. Summary of results.

Please note: Wiley-Blackwell are not responsible for the content or functionality of any supporting materials supplied by the authors. Any queries (other than missing material) should be directed to the corresponding author for the article.